Solar Energy 262 (2023) 111826

Contents lists available at ScienceDirect

Solar Energy

journal homepage: www.elsevier.com/locate/solener

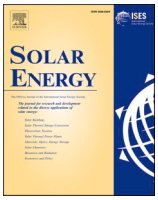

A methodology to assess the dynamic response and the structural performance of floating photovoltaic systems

Rubén Claus, Mario López *

DyMaSt Research Group and Dept. of Construction and Manufacturing Engineering, University of Oviedo, Polytechnic School of Mieres, 33600 Mieres-Asturias, Spain

ARTICLE INFO

Keywords:
Solar energy
Photovoltaics
FPV
Floatovoltaics
Numerical modelling

ABSTRACT

This study presents a comprehensive methodology for evaluating floating photovoltaic (FPV) structures, focusing on the impact of wind and wave conditions from hydrodynamic and structural perspectives. The methodology is applied to a Class 1 pontoon-type structure with rigid and hinged configurations. A total of 558 simulations are conducted, considering various environmental actions, configurations, and mooring line chain sections. The results provide essential data on loads and motion time series for subsequent structural analysis. Wind forces primarily influence surge and sway motions, while wave forces dominate other motion components. Comparing the hinged configuration to the rigid one, a significant reduction in maximum yaw motions of 32% to 76% was observed, depending on the mooring chain section employed. This reduction in yaw motions may positively impact the energy yield. However, an inverse trend was observed for pitch motions. Hence, a comprehensive assessment of wave-induced motions is crucial for selecting the optimal FPV configuration. Furthermore, heavier chain sections effectively limited surge, sway, and yaw motions, with variations of up to 75% observed in the hinged configuration when comparing different chain options. Structural analysis highlights the importance of wave characteristics, mooring system configuration, and system flexibility. The findings emphasize the need to consider environmental conditions, structural aspects, and energy efficiency in optimizing FPV configurations.

1. Introduction

1.1. Floating photovoltaic systems overview

Solar photovoltaic (PV) energy is projected to become the dominant renewable energy source soon. Its potential to meet global energy demand, coupled with the decreasing costs of PV technology, has contributed to this forecast [1]. Floating PV systems (FPV) established on inland water bodies have exhibited remarkable growth over the past decade, with an impressive annual growth rate of 133% [2]. These systems offer several advantages, which are outlined below:

- Large-scale ground-mounted PV (GPV) systems require substantial land areas, leading to conflicts with various land uses, including agriculture, recreation, mining, and infrastructure development. FPV systems can help mitigate these conflicts [3].
- The water cooling effect can potentially improve the efficiency of PV modules [4], although the extent of this effect is still not well

Abbreviations: A_{ref}, Reference area [m^2]; BEM, Boundary element method; CFD, Computational fluid dynamics; CoG, Centre of gravity; C_D, Drag coefficient [-]; C_L, Lift coefficient [-]; C_M, Inertia coefficient [-]; C_S, Sheltering coefficient [-]; D, Characteristic dimension of a structural element [m]; DoF, Degree of freedom; FEM, Finite element method; FPV, Floating Photovoltaic; FRP, Fibre-reinforced polymers; F_{wav}, Wave force [N]; F_{wd}, Wind drag force [N]; F_{wl}, Wind lift force [N]; $\mathbf{f}$, total forces and moments vector [N or Nm]; $\mathbf{f}_c$, connection forces and moments vector [N or Nm]; $\mathbf{f}_d$, diffraction forces and moments vector [N or Nm]; $\mathbf{f}_F$, Froude-Krylov forces and moments vector [N or Nm]; $\mathbf{f}_g$, Gravitational forces and moments vector [N or Nm]; $\mathbf{f}_h$, Hydrostatic forces and moments vector [N or Nm]; $\mathbf{f}_M$, Morison forces and moments vector [N or Nm]; $\mathbf{f}_r$, Radiation forces and moments vector [N or Nm]; $\mathbf{f}_w$, Wind forces and moments vector [N or Nm]; H, Wave height [m]; HDPE, High-density polyethylene; h, Water depth [m]; L_e, Element size [m]; $\mathbf{M}$, Structural mass matrix [kg]; PV, Photovoltaic; S_w, Wind-exposed surface [m^2]; T, Wave period [s]; t, Time [s]; U, Wind Speed [m/s]; U_{10}, Mean wind speed averaged for 10 min; u, Flow velocity [m/s]; V, Volume of a body [m^3]; $\mathbf{X}$, Cartesian coordinate system [m]; $\mathbf{x}$, Position matrix [m]; z, Height above the ground or ocean surface [m]; z_{ref}, Reference height above the ground or ocean surface [m]; α, Terrain roughness [-]; γ, Surface roughness coefficient [-]; λ, Wavelength [m]; Θ, Wave propagation direction [deg]; ρ, Fluid density [kg/m^3]; Φ, Velocity potential [m^2/s]; Φ, Velocity potential expressed as a function of the spatial coordinates [m^2/s]; ω, Angular frequency [rad/s].

* Corresponding author.
E-mail address: mario.lopez@uniovi.es (M. López).

https://doi.org/10.1016/j.solener.2023.111826
Received 29 March 2023; Received in revised form 26 May 2023; Accepted 25 June 2023
Available online 8 July 2023

understood [5]. The higher wind speeds experienced over water bodies also contribute to the cooling effect [6].
- Regular cleaning of PV modules is ensured due to the presence of water [7].
- The nature of water bodies minimizes shadows cast on the PV modules [8].
- Evaporation losses in water reservoirs are reduced [9].
- Excessive algae growth is prevented [10].
- Synergies with hydroelectric plants are possible [11].

However, it is important to note that the installation and maintenance costs of FPV systems are still higher than those of GPV plants [12]. Furthermore, the potential expansion of FPV applications on freshwater is limited by the available surface area of existing water bodies. Seasonal variations in water levels further restrict their suitability, especially in the case of artificial dams [13]. As a result, there has been a proposal to explore the solar resource on the vast and unoccupied ocean surface through the deployment of marine FPV systems [14]. Marine FPV systems offer the potential for strong synergy with other marine activities [15], and can play a significant role in decarbonizing the shipping industry [16].

FPV installations typically consist of the following key components: PV modules for capturing solar energy, floats for buoyancy, optional support structures for the PV modules, a mooring and anchoring system, and the necessary electrical components and storage systems. Over time, various typologies of FPV systems have been successfully commercialized, with many others currently in development or proposed for future implementation. While different criteria can be used to classify these typologies, the structural arrangement is widely acknowledged as one of the most prominent and influential factors in differentiating FPV systems (Fig. 1) [17].

1.2. State-of-the-art in FPV structure design

Despite the recent advances in FPV systems, to date, only a recommended practice on the design, development, and operation of freshwater plants has been published [19]. There are no specific standards nor well-established design methodologies to assess the survivability of FPV systems against rough environmental conditions. Various models are being applied to analyse and design FPV systems, which can be grouped into loading models, response models, and structural models.

Among the different types of loads, the environmental ones – mainly wind, waves and currents – are the most hindering aspect of FPV design [20]. These loads are commonly estimated using analytical or numerical methods. Analytical methods involve the use of semi-empirical linear models, such as the Morison formula [21,22], and the Maruo formula [23] for wave loads, as well as generic formulae for wind loads. These methods require empirical coefficients, which can be obtained from recommended practices and codes (e.g., [22–26]), or through experimental testing in wave tanks or wind tunnels (e.g., [23,27]). Numerical methods, specifically Computational Fluid Dynamics (CFD), are capable of simulating the dynamic and non-linear nature of the environmental loads, albeit with a higher computational cost. Several authors have employed CFD approaches to model wind loads on FPV structures [28–31]. However, for a balance between computational efficiency and accuracy, wave loads are often obtained using models based on the potential flow theory and the Boundary Element Method (BEM) [32–36].

The design of the FPV system influences its conversion efficiency, as the movements of the floating body can cause variations in tilt and azimuth angles. Although these changes may be insignificant in freshwater and small bodies of water, reductions in insolation of up to 2.52% have been reported in offshore FPV systems [37]. The study also indicated that pitch variations may have a greater impact compared to yaw and roll. Therefore, conducting response analysis is crucial, not only for the structural design but also for accurately estimating the energy yield of the system.

The response model of a FPV plant can be either static or dynamic. In a static response model, loads are applied slowly, and inertial forces are not relevant. Although wind and wave loads are usually estimated with analytical methods [21–23,34], these environmental loads can also be

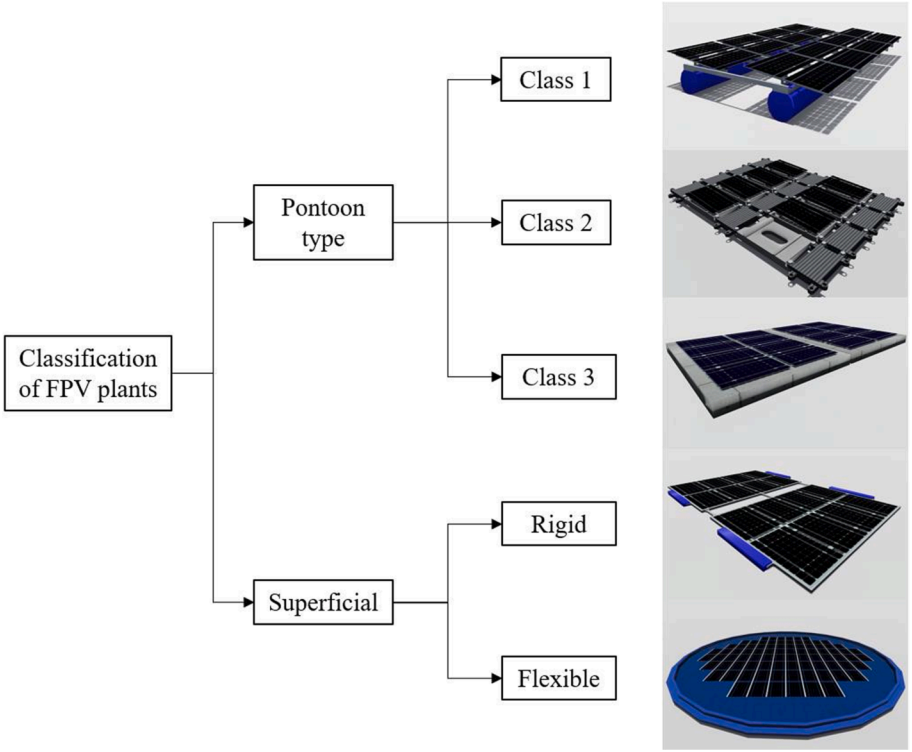

Fig. 1. Classification of FPV systems (based on references [17,18]).

simulated through displacement loads [24], or CFD [29], providing alternative approaches for their modelling. The behaviour of the FPV system is usually assessed as a single 3D rigid body, but it can also be evaluated as a group of independent, yet connected, rigid bodies [34,35]. The rigid body dynamics analysis of a FPV design can be performed in the frequency [31–35] or time domain [38,39]. Depending on the geometry and the boundary conditions, the dynamic response may be simplified through a 2D approach [36].

For the structural analysis of FPV systems, the Finite Element Method (FEM) is widely used, although classic analytical methods can be used for beams and slender FPV structures [33,38]. FEM analysis can be static or transient, depending on the importance of the inertia effects. For a static response of a FPV structure, a static FEM analysis is usually performed (e.g. [22,24,29,40]). A static analysis may also be performed for a single time step of a rigid solid dynamic analysis, if the structural deformation and stress variations are sufficiently small. The FEM model is commonly independent from the dynamic analysis, but the loads and boundary conditions are retrieved from the latter. The same approach may be adopted for a transient FEM model [31], which can be coupled with a dynamic response model in a hydroelastic analysis. Although hydroelasticity is preferable in the design of flexible FPV systems, which have been recently studied for the marine environment [41–43], it has been applied to analyse rigid and pontoon-type designs with a specific focus on the fluid–structure response [44], as well as the structural analysis [45,46]. Nonlinear 2D models for strong hydro-elastics have also been proposed to analyse FPV structures [47,48]. However, hydroelastic models present a very high computational cost for design and engineering purposes.

1.3. Aims and scope

The review of the literature reveals the absence of standardized methodologies for analysing the complex and diverse nature of FPV structures, presenting a significant challenge in the field. Existing studies have focused on specific aspects, resulting in a fragmented understanding of FPV systems. Furthermore, the differentiation between rigid and flexible systems has necessitated distinct approaches. Thus, there is an urgent need for a comprehensive and standardized procedure to effectively analyse and optimize the performance of FPV systems.

This article addresses this gap by presenting a significant contribution in the field of FPV systems. It introduces a standardized procedure that integrates hydrodynamic and structural analysis for both rigid and flexible designs, aiming to establish a comprehensive methodology for understanding and enhancing the performance of FPV systems.

The study primarily focuses on a pontoon-type FPV system and systematically investigates its response under various wind and wave conditions. Two configurations, rigid and hinged, are considered, providing valuable insights into their influence on the design of FPV structures. Additionally, three different sections of mooring chains are analysed to further enhance the understanding of their impact on the system.

To achieve a comprehensive analysis, the study combines hydrodynamic and structural analysis. Rigid body dynamics are employed to model the system's response, while a combination of BEM and semi-empirical formulae is used to estimate the loads. In the case of the hinged configuration, a multibody approach is adopted to accurately capture the behaviour of the system. The positions, velocities, and accelerations obtained from the response model serve as inputs for subsequent structural analysis using the FEM. This integrated approach allows for a thorough assessment of the FPV structure, optimizing the mooring lines and evaluating the main structural components.

1.4. Organization of the paper

The remainder of this paper is structured as follows. In section 2, the methodology is illustrated and disclosed. The analysed FPV and its configurations are described, the environmental conditions and their combination are defined, and the applied numerical model is explained. In section 3, results are presented and discussed in the form of motions, forces acting on the structure, mooring line forces, and forces and stresses in the structural elements. In section 4, conclusions are drawn and discussed.

2. Materials and methods

2.1. General methodology

The proposed methodology for the design of FPV systems is illustrated in Fig. 2. It begins with the estimation of environmental loads, which can be achieved using analytical formulations or numerical methods. Considering that most FPV systems require a dynamic response model, a rigid body dynamics approach is required to assess the position, velocity, acceleration and forces acting on the FPV structure. This analysis assumes small deformation under the applied forces and excludes structures that display fluid, highly elastic or plastic behaviour, making it unsuitable for flexible FPV designs (Fig. 1). As the response analysis may influence the boundary conditions of the loads acting on the body, the loading and response models are analysed altogether. Once the response of the structure is obtained, a subsequent structural analysis and optimization are conducted. The stages of this methodology are disclosed hereafter.

First, the geometry of the FPV system is numerically modelled as an assembly of either slender 1D bodies or diffracting 2D bodies, depending on their characteristic size (D) with respect to the wavelength (λ) of the considered waves (Fig. 3). If $D/\lambda < 0.05$, the prevailing forces are drag and/or inertia and the element is considered slender (wave force regimes I, II and V in Fig. 3). Thus, it is modelled by a 1D body for which appropriate drag coefficients (C_D) and inertia coefficients (C_M) should be defined. If $D/\lambda > 0.05$, the prevailing forces are diffraction and radiation, and the structure is considered a large volume element (wave force regimes II and IV in Fig. 3). This element is thus modelled by means of diffracting panels. If both diffraction and drag forces are relevant, drag coefficients may be assigned to the diffraction bodies as well. The FPV components that do not interact with the water (e.g. the PV modules) are modelled by means of mass points and aerodynamic coefficients. The first summarizes the mass and inertial properties of the component and the second provides information required to estimate wind loads.

Once the hydrodynamic model is defined, if the FPV structure has diffracting elements, a frequency domain rigid body analysis is carried out. This is performed through potential flow theory assuming an ideal fluid, and irrotational flow. This theory is approached through different numerical methods, with the three-dimensional panel methods being the most extended among them [49]. This analysis describes the linear behaviour of floating bodies against regular waves for a defined range of wave frequencies and directions. Certain nonlinear effects, such as cable dynamics, wind drag, or forces on slender elements, can be incorporated into the analysis after linearization. The motion of the fluid around the modules is defined by the velocity potential:

$$\phi(\mathbf{X}, t) = Re[\varphi(\mathbf{X})e^{-i\omega t}] \quad (1)$$

where: t is the time, ω is the angular frequency and φ is the velocity potential expressed as a function of the spatial coordinates.

If diffracting elements are not included in the design, the frequency domain analysis can be skipped. Instead, a time domain analysis is performed, which requires defining the design environmental conditions.

The wind action is characterised by the wind speed (U) as well as its time and spatial variability. For short-term stationary wind conditions, the mean wind speed is often used as a rough estimate of wind intensity. For a more accurate analysis it is possible to use a wind speed spectrum, which considers the variations in wind speed over time. Additionally,

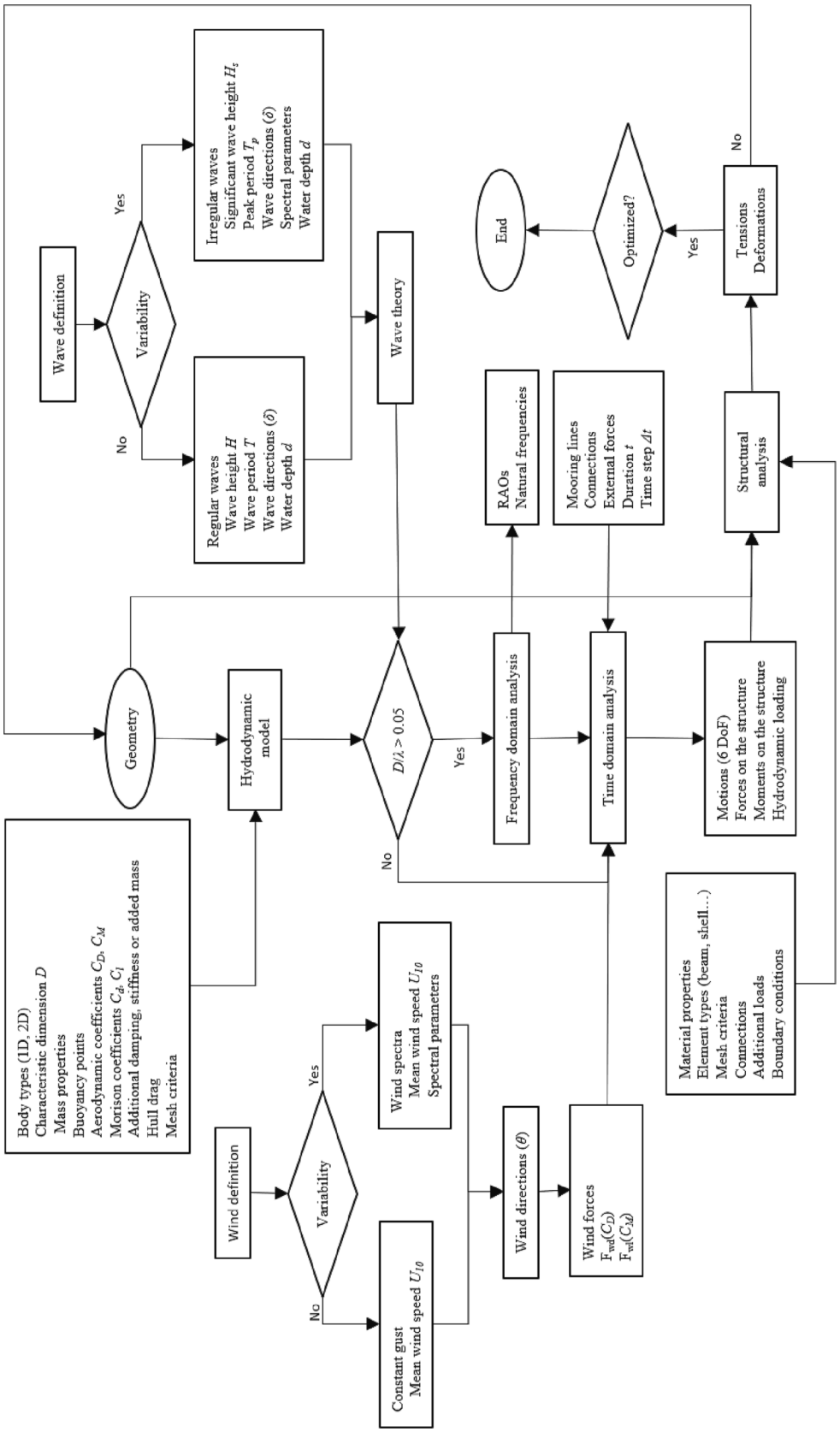

Fig. 2. Proposed methodology layout for the design of FPV systems.

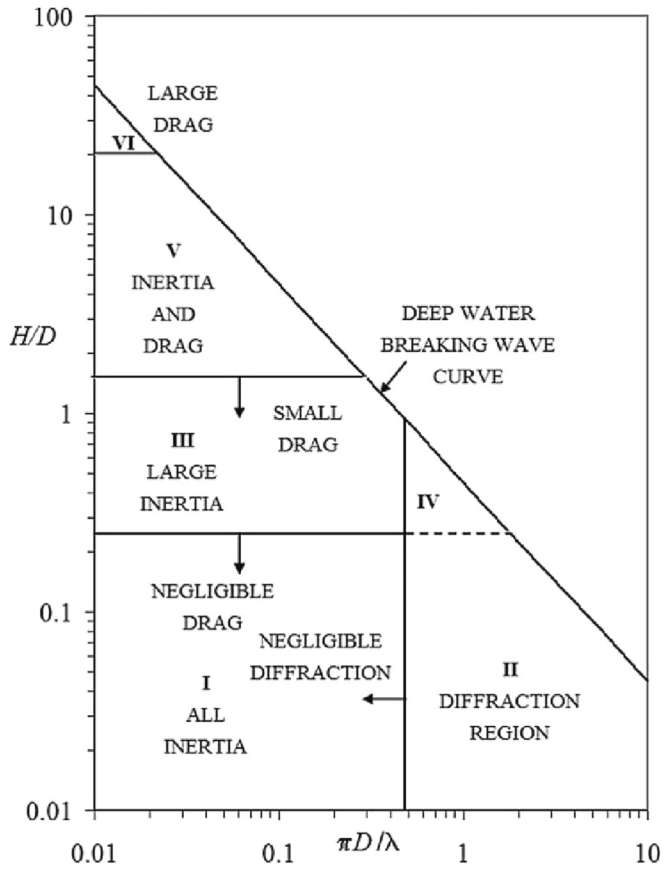

Fig. 3. Wave force regimes according to [50].

direction variations in the wind gust can be considered to capture the full range of wind behaviour. The mean wind speed U_{10} is commonly measured at a reference height of $z_{ref} = 10$ m and usually needs to be adjusted to the height of the PV modules or the freeboard of the FPV structure through a wind profile model, such as the power law:

$$U(z) = U_{10}\left(\frac{z}{z_{ref}}\right)^{\gamma} \tag{2}$$

where γ is the surface roughness coefficient.

Waves are generally characterized by the wave height (H) and the wave period (T) as well as their time and spatial variability. The Airy wave theory is widely used and considered the simplest approach. However, depending on the water depth and the wave climate at the FPV plant site, a different theory could be more suitable (Fig. 4).

Regular wave conditions are suitable for the preliminary design of a FPV plant. However, for an accurate design, irregular wave conditions and non-linear wave theories should be considered. The irregular wave conditions (i.e., their short-term variability) can be defined in terms of a parametric model such as the Pierson-Moskowitz spectrum and the JONSWAP spectrum [25]. Again, direction variations can also be accounted for through directional spreading functions.

Once the frequency domain analysis is completed, the next step is the time domain solution. The motion of the FPV system can be described in the time domain as follows:

$$\mathbf{M}\cdot\ddot{\mathbf{x}}(t) = \mathbf{f}_h(t) + \mathbf{f}_F(t) + \mathbf{f}_d(t) + \mathbf{f}_r(t) + \mathbf{f}_M(t) + \mathbf{f}_c(t) + \mathbf{f}_m(t) + \mathbf{f}_w(t) \tag{3}$$

with: $\mathbf{x}(t)$, the position of the floating body; $\mathbf{f}_h(t)$, the hydrostatic force; $\mathbf{f}_F(t)$, the Froude-Krylov forces; $\mathbf{f}_d(t)$, the diffraction forces; $\mathbf{f}_r(t)$, the radiation forces; $\mathbf{f}_M(t)$, the Morison forces; $\mathbf{f}_c(t)$, the connection forces; $\mathbf{f}_m(t)$, the mooring forces and $\mathbf{f}_w(t)$, the wind forces.

The Morison forces are obtained through the Morison equation [52],

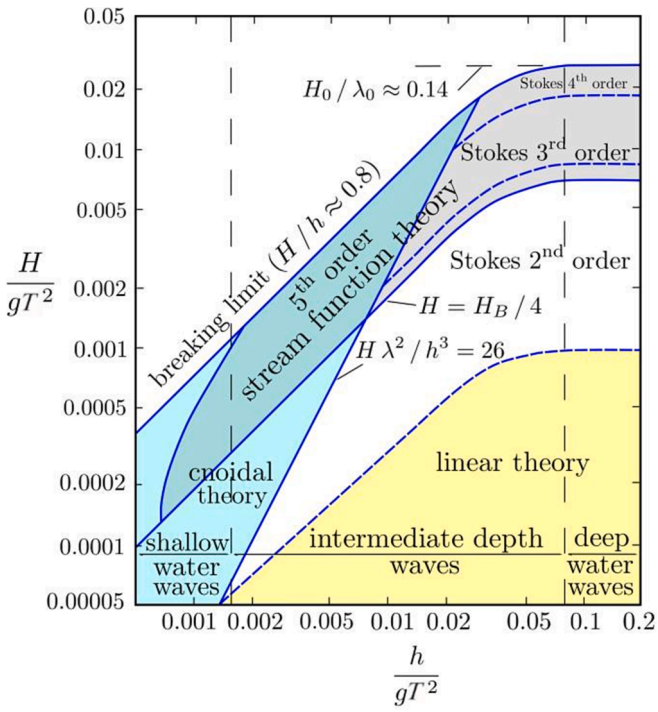

Fig. 4. Ranges of applicability of several wave theories. Adapted from [51].

that reads as follows:

$$F_{wav} = \frac{1}{2}\rho C_D A_{ref} u|u| + \rho V C_M \dot{u} \tag{4}$$

where ρ is the fluid density, C_D is the drag coefficient, C_M is the inertia coefficient, V is the volume of the body, u is the flow velocity and A_{ref} is its reference area.

The connection forces $\mathbf{f}_c(t)$ are those transferred between connected floating bodies. These result from the restriction of DoFs the connection establishes and are computed through the stiffness of the connection and the relative motions of the involved floating bodies. The mooring forces $\mathbf{f}_m(t)$ are those transferred by the endpoint of the mooring line to the floating structure. The mooring lines are slender elements subject to gravitational forces, buoyant forces, structural inertia forces, radiation forces, drag forces, as well as tensions and bending moments.

The wind forces $\mathbf{f}_w(t)$ are estimated through an analytical approach. Most analytical expressions contemplate the dynamic nature of the environmental actions through parameters and simplify the estimation of loads through a static approach [23]. In the case of FPV plants, wind loads should be considered on the PV panels and any other relevant exposed elements. The forces on the structure due to a steady wind load can be divided into drag forces F_{wd} and lift forces F_{wL} and estimated through the following formulae [26]:

$$F_{wd} = \frac{1}{2}\rho C_d C_s S_w U^2 \tag{5}$$

and

$$F_{wl} = \frac{1}{2}\rho C_l C_s S_w U^2 \tag{6}$$

where C_d is the drag coefficient, C_l is the lift coefficient C_s is the sheltering coefficient, and S_w is the wind-exposed surface. Specific drag and lift coefficients for FPV structures are not available in the specifications and therefore should be obtained through numerical and/or experimental testing, especially in the case of complex shapes. In the time domain analysis, if the boundary conditions of the FPV structure vary

over time, so does the wind force, even if the wind gust is constant in intensity and direction. This is because the values of C_d, C_l and S_w vary if the FPV structure rotates in any of its degrees of freedom. Note that, in this methodology, dynamic effects such as vortex shedding, galloping or flutter are not accounted for.

Once all the forces are obtained for a time step, the dynamic problem can be solved through the integration of Equation (3). This is performed through a 2-stage predictor–corrector algorithm. In the first stage, the forces on the structure are calculated as a function of time, position, and velocity. The position and velocity of the floating body for the next time step are then predicted in accordance with those forces. In the second stage, forces are obtained again as a function of the new values of time, position, and velocity. Then, the velocity and position are corrected through Taylor's theorem. The structure adopts its new position, and the algorithm starts over.

Upon completion of the time domain analysis, results may be retrieved in the form the motions and forces acting on the structure for the complete time series. These forces are the input for the subsequent structural verification. This analysis can be static or dynamic and can be carried out through a FEM model. For this methodology, since deformations are assumed sufficiently small, a static analysis is performed for each time step of the simulation. For a complete analysis, a FEM model with a specific modelling and meshing strategy is required. The boundary conditions for the static FEM analysis of a moving floating structure should provide sufficient, yet minimal constraints to prevent rigid body motions. To do so, the rigid body motions should be balanced by inertial forces with minimum constraints. This can be referred to as inertial relief, where the applied forces and torques are precisely balanced by the inertial forces induced by the previously computed acceleration field. The 3-2-1 constraint principle may be applied to properly define the constraint points [53]. After the analysis, the reaction forces in these points must be checked, to verify they are sufficiently small when compared to the applied forces.

2.2. Pontoon-type FPV design

The studied technology is a Class 1 pontoon-type FPV design, partially based on the design proposed by Lee et al. [45]. The raft can hold up to 70 crystalline silicon PV panels with a 30° inclination and covers a total horizontal area of 36 × 7 m^2 (Fig. 5). This floating plant consists of 10 rows of cylindrical floats connected and aligned by 18 main beams and held in place by a mooring system. The spacing of the floats of the plant is 4 m while the module row spacing is 2.27 m. The PV panels are installed over the cylinders through a supporting structure. This plant has been analysed for two configurations: i) a rigid plant with continuous main beams and ii) a multi-float assembly, achieved through 4 hinged connections. These connections divide the FPV plant into 5 independent floating modules, each consisting of two rows of floaters. Each module is able to float independently and is connected to the contiguous one through a flexible connection, which is an approach that has been adopted in real-field applications [54]. This connection system behaves as a bending moment free system on the fluctuating water surface and has been already applied in other FPV designs [40]. Note that, since the applied methodology accounts for float interactions in

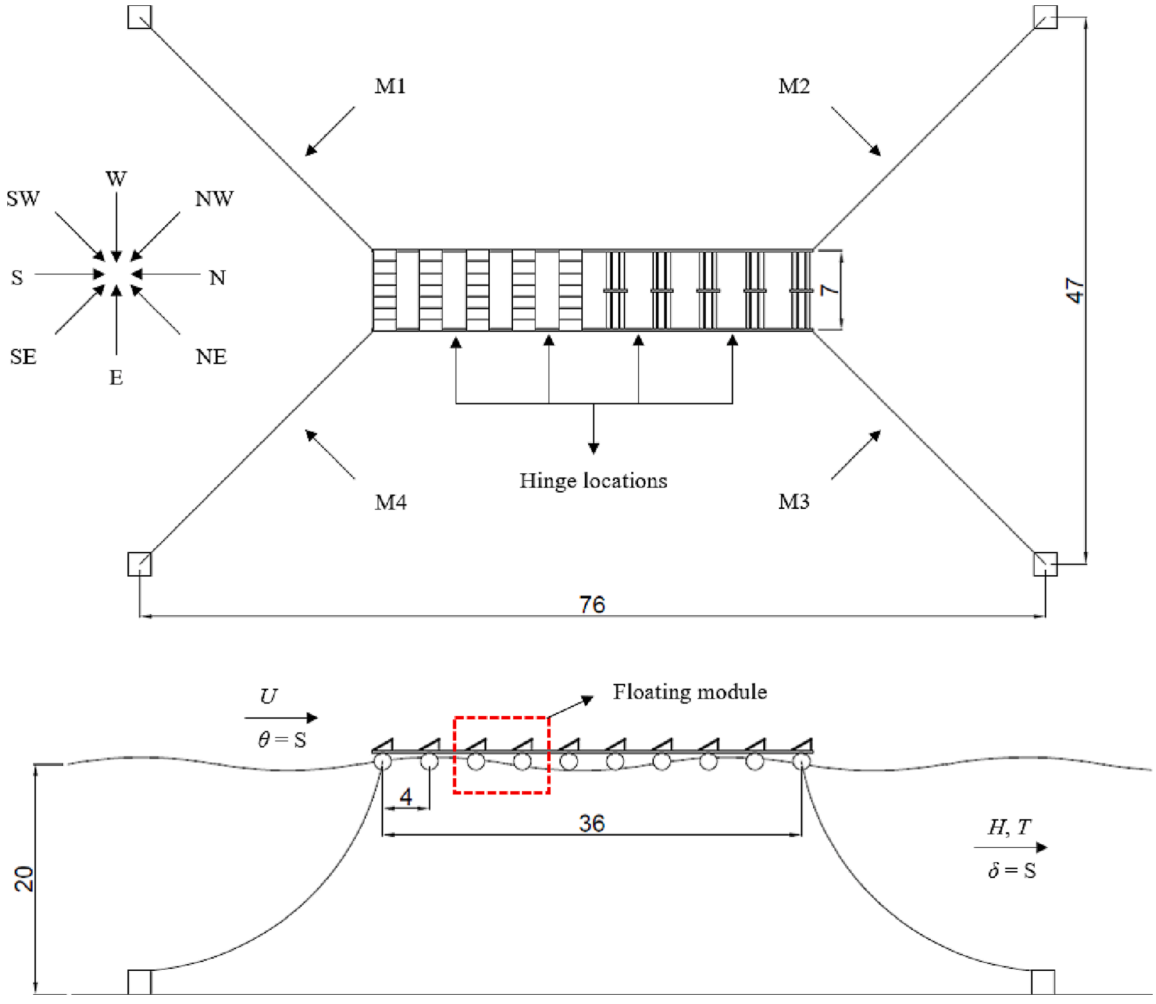

Fig. 5. Schematics of the pontoon-type FPV design and environmental actions. Measurements in m.

multi-body assemblies, it could be considered to assess Class 2 FPV plants.

Based on the design proposed by Lee et al. [45], the floats are made of high-density polyethylene (HDPE) pipes and the supporting structure is constructed from fibre-reinforced polymer (FRP), which offers low density and high corrosion resistance. The mechanical properties of the HDPE pipes and the FRP are summarized in Table 1 (retrieved from [55;45], respectively).

The structure is kept in place by a mooring system consisting of 4 catenary lines tied to each corner of the arrangement. Each mooring line has a total length of 40 m and is anchored to a fixed point in the seabed. Three different mooring line sections were adopted to perform an optimization of the mooring system (Table 2, [56]).

2.3. Test conditions

This design was analysed for a generic environment defined by a constant wind gust and regular waves modelled through the Second Order Stokes wave theory (Fig. 4), both coming from multiple directions, and a constant water depth, *d*.

This design was tested for 558 different scenarios, resulting from combining:

- 5 environmental parameters: wind speed, wind direction, wave height, wave period and wave direction (Fig. 5). Due to the nature of the environmental loads, wind and waves were not combined in opposing directions.
- 2 FPV configurations: rigid and hinged (Fig. 5).
- 3 chain sections, namely: Chain 1, Chain 2 and Chain 3 (Table 2).

The values considered for each parameter are summarized in Table 3.

The wind loads were analytically estimated through Equation (5) and Equation (6). The required wind speed corresponds to the height of the PV modules, which stands about 1 m above the water level. Applying Equation (2) and a surface roughness $\gamma = 0.12$, the wind speed at the height of the panels is $U\ (z = 1\ \text{m}) = 20$ m/s. The wind forces were estimated for the surface of the PV panels (S_w), since the contribution of the exposed freeboard of the floats or the FRP members was considered negligible.

Drag and lift coefficients were adopted from a previous experimental study performed by You et al. [27] and are summarized, for each wind direction, in Table 4. Sheltering coefficients were adopted from Ikhennicheu et al. [23] and are summarized in Table 5.

2.4. Methodology implementation

The proposed methodology was applied to the FPV design described in section 2.2 by means of different numerical environments. The frequency-domain and time-domain hydrodynamic response analyses were solved in Ansys Aqwa Line and Aqwa Naut, respectively. Aqua Naut was used since it allows solving the time-domain response of floating structures and their mooring system by including nonlinear Froude-Krylov and hydrostatic wave forces on the instantaneous wetted surface, which is relevant considering the relative dimensions of the FPV system to the minimum considered wavelength ($\lambda = 39$ m). This approach has already been implemented with success to study other multi-body floating structures, and more details can be found previous studies (*e.g.* [57]).

The floats of the FPV system were modelled as 2D diffracting elements (since $D/\lambda > 0.05$), whereas the beams and mooring lines were modelled as 1D Morison elements (since $D/\lambda < 0.05$). The cylinders were meshed through 17,152 quadrilateral elements, of which 8,571 were considered diffracting, with an element size of $L_e = 0.2$ m (Fig. 6). Each test case had a time step of 0.01 s and a duration of 500 s.

The mesh size is sufficiently small when compared to the minimum wavelength of the considered wave conditions ($7L_e < \lambda$). The values adopted for the Morison coefficients were $C_D = 0.75$ and $C_M = 2$, which are standard values for a cylinder tube [58]. The beams of the structure were modelled as rigid elements, whereas the mooring lines were modelled as a concatenation of spring elements with a longitudinal drag coefficient of $C_D = 0.025$. The mass and inertia of the cylinders as well as the PV modules and secondary members were modelled through 5 mass points, each associated to every floating body in the hinged

Table 1
Geometry and mechanical properties of the floats and beams. Source: [55] and [45].

Property	Floats	Beams
Length (m)	7	4
Section dimensions (mm)	Circular (Ø1000 w30)	I (150 × 150 × 10)
Section (cm^2)	914	43
Inertia (mm^4)	1.6×10^{10}	1.7×10^7, 5.6×10^6
Material	HDPE	FRP (polyester + E-glass)
Density (kg/m^3)	960	1800
Young's module (GPa)	1.25	30.76
Poisson's coefficient	0.4	0.3
Tensile yield strength (MPa)	33	415.3

Table 2
Geometry and mechanical properties of the catenary chain sections. Source: [56].

Property	Chain 1	Chain 2	Chain 3
Length (m)	40	40	40
Linear density (kg/m)	2.2	5.2	10
Equivalent section (cm^2)	2.8	6.6	12.8
Equivalent diameter (mm)	18	29	40
Material	Steel	Steel	Steel
Break load (kN)	50	132	251

Table 3
Possible values for the environmental parameters considered.

Parameter	Test values
Wind speed, U_{ref} (m/s)	0, 30
Wind direction, θ	N, NE, E, SE, S, SW, W, NW
Wave height, H (m)	0, 0.5, 1
Wave period, T (s)	5, 7
Water depth, d (m)	20

Table 4
Drag and lift coefficients for different wind directions. Based on [27].

Wind direction	C_d	C_l
N	0.6	0.5
NE	0.4	0.5
E	0.1	0.0
SE	0.3	−0.5
S	0.5	−1.0
SW	0.3	−0.5
W	0.1	0.0
NW	0.4	0.5

Table 5
Sheltering coefficients for the rows of PV modules. Based on [23].

Row	C_S
First	1.0
Second	0.4
Third	0.3
Rest	0.1

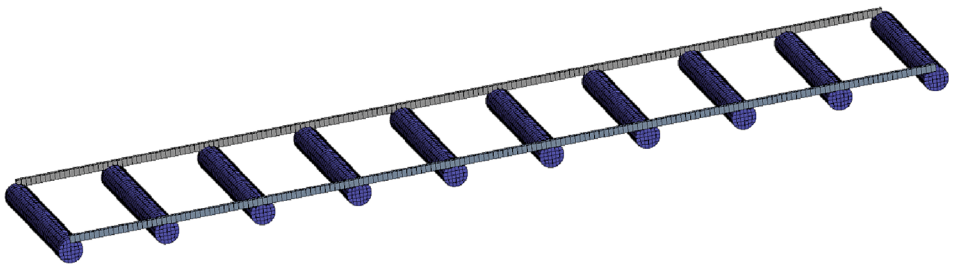

Fig. 6. Meshed floats and main beams of the pontoon-type FPV.

configuration and merged into one in the rigid assembly. The independent floating modules in the hinged configuration are connected through pairs of hinges, located at the centre of the beams that connect the floating modules. These connections restrict all DoF except rotations around the axis of the floating cylinders. Aerodynamic coefficients were assigned to each floating body, according to the parameters previously specified in Table 4 and Table 5.

The structural analysis of this FPV design was performed through a FEM model, using Ansys Mechanical. Levels of stress were obtained for the floats, which were modelled as shell elements, and the main beams, which were modelled as beam elements. The floats were meshed through 10,320 mostly quadrilateral elements, while the beams were discretized into 486 elements. The 3-2-1 method was used as a boundary condition and inertia relief was applied. The hydrodynamic loads were imported from the time domain BEM analysis, and the wind forces and the forces of the mooring lines were applied as external forces. The PV modules were again modelled as external mass points.

3. Results and discussion

3.1. Response analysis

Results from the hydrodynamic response analysis were obtained in the time domain in the form of motions (6 DoF) and forces on both the floating structure and its mooring system. These results were registered for all the test cases and were used as inputs of the subsequent structural verification. To better illustrate the findings of this analysis, a test case is disclosed as an example. Then, the motions of the floating structure and the overall environmental forces acting on it, as well as the test cases that led to them, are summarized and discussed.

A mesh sensibility analysis was carried out to ensure the independence of the results from the mesh. Several control values (maximum wave force on the floats, maximum force on M1 and maximum surge motion) are plotted against the number of diffracting elements in Fig. 7, for the wave scenario that registered the highest wave forces ($H = 1$ m, $T = 5$ s, $\theta = S$ and the rigid configuration). As shown, the mesh refinement did not affect the control values.

Fig. 8 shows an example of the motions of the FPV structure and the forces on the mooring system for the rigid configuration and Chain 3.

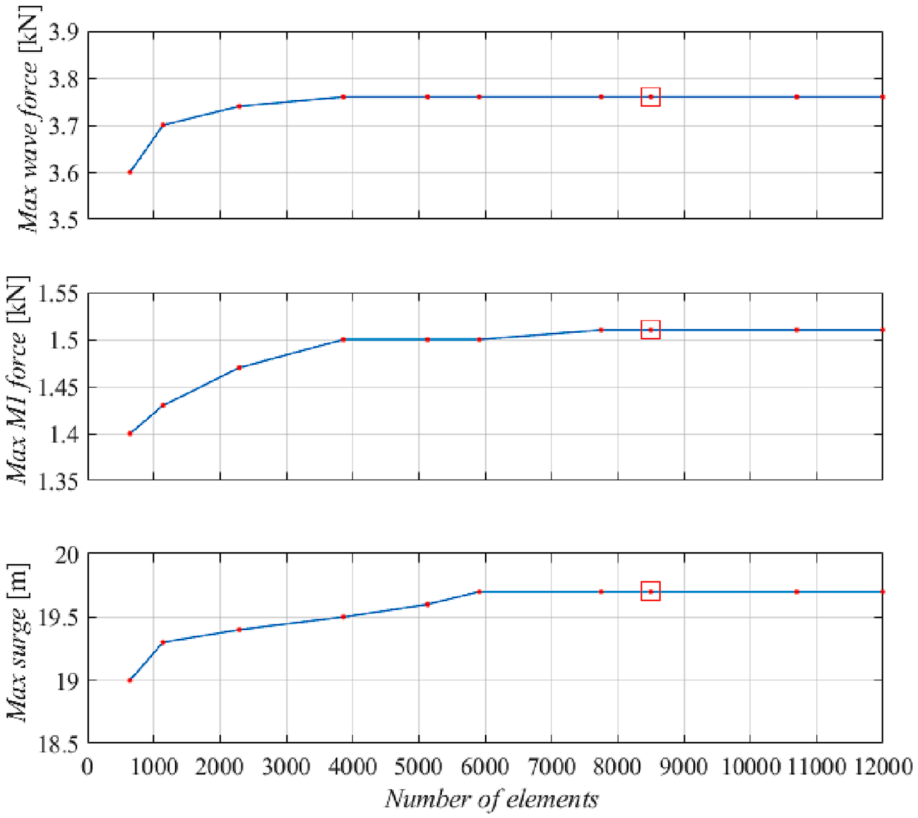

Fig. 7. Mesh sensibility analysis for $H = 1$ m, $T = 5$ s and $\theta = S$. The square marker represents the selected number of elements.

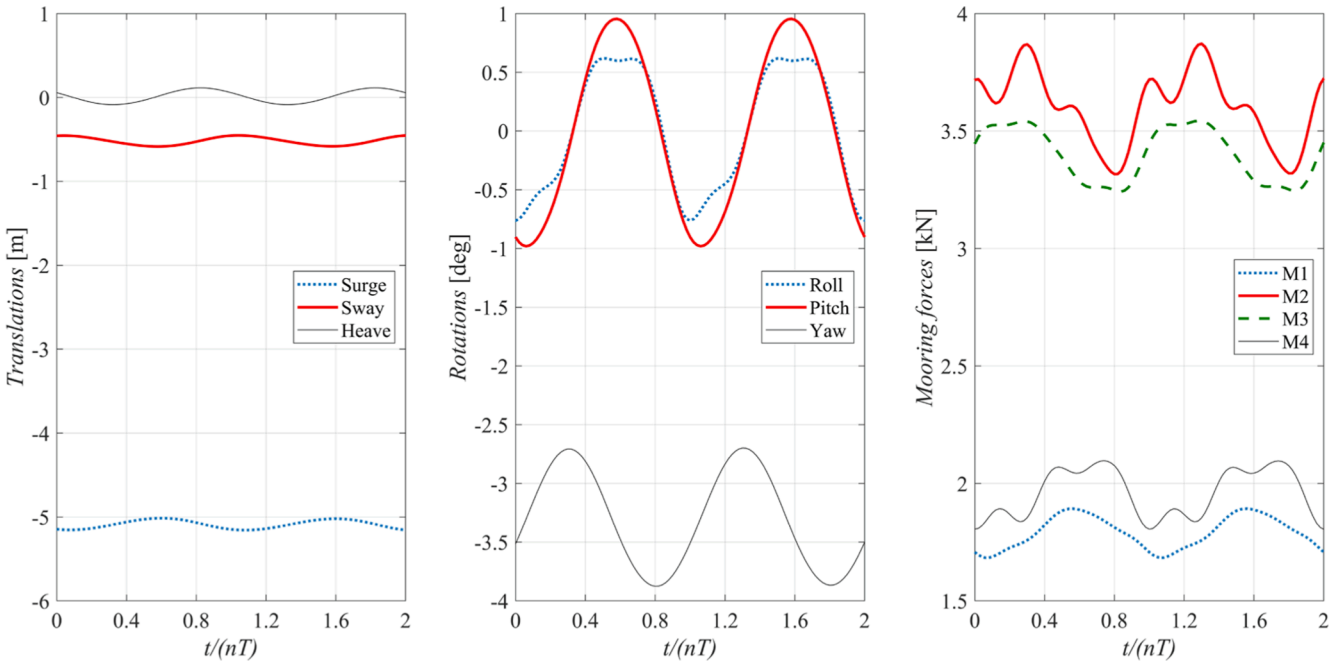

Fig. 8. Example of motions and mooring forces of the FPV plant (environmental conditions: $H = 0.5$ m, $T = 5$ s, $U = 30$ m/s, $\theta =$ N and $\delta =$ NW).

For clarity, only a short time of the simulation after the ramping period is displayed (note that the obtained response is harmonic). Motions are shown with respect to the centre of gravity of the floating structure and the surge direction corresponds to the N direction according to Fig. 5.

The maximum 6-DoF motion amplitudes of the device (measured as variations of the CoG of the structure with respect to its starting position) for all the analysed conditions with $H = 1$ m are shown in Fig. 9.

In terms of translational motions, the largest surge motions were observed when the wind and waves were aligned in the N direction. This outcome was anticipated due to the N direction having the highest wind drag coefficient. The wind force is the primary contributor to this displacement. It is worth noting that the motion was limited using heavier chain sections, while both hinged and rigid configurations exhibited similar results.

As for the maximum sway motions, they occurred in the test case where waves from W and wind from NW (and their symmetric counterparts) were present. This is because the wind drag coefficient for the NW direction was higher than that of the SW or W directions. Furthermore, the sway motions were weakly dependent on the wave direction since the main driving force was the wind. Sway motions are also limited by using heavier chain sections.

The heave motions demonstrated similarities across all test cases involving waves, irrespective of the wave direction. Wind exerted minimal influence on the heave motions, and neither the chain section nor the FPV configuration had a significant impact on them.

Regarding rotational motions, the maximum roll values were registered for side waves (W or E directions according to Fig. 5) and N wind. In this case, the waves were the main contribution to this motion, as

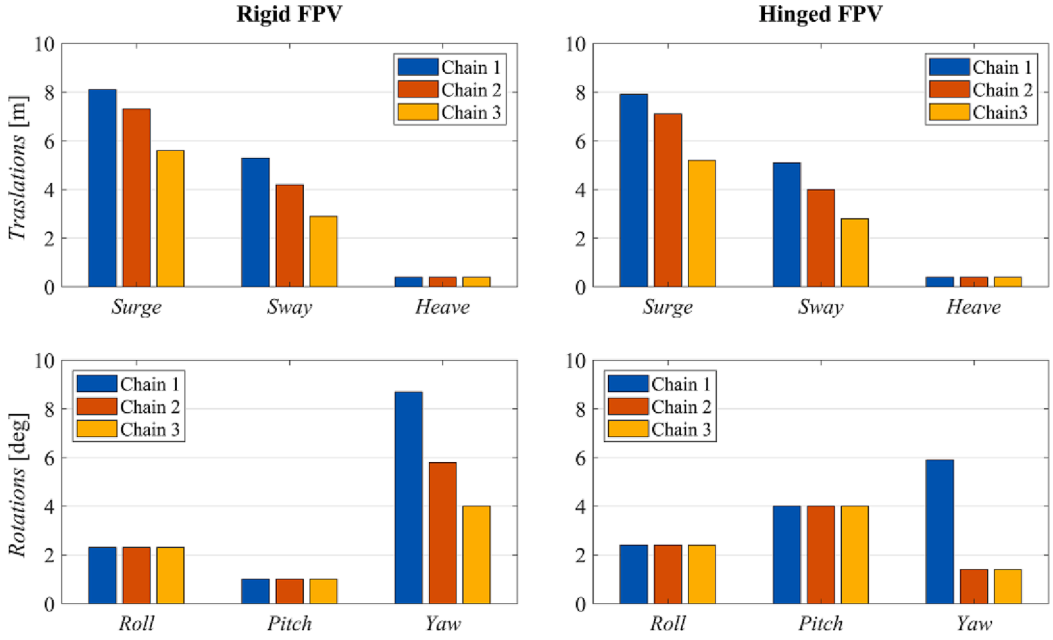

Fig. 9. Maximum motions of the FPV plant for $H = 0.5$ m. Note that, for the hinged configuration, the maximum values were gathered for every floating body.

similar values were achieved in the absence of wind. Both rigid and hinged configurations exhibited similar behaviour in terms of roll.

The highest pitch motions were observed when waves originated from SW, although comparable values were observed for wave directions with a N or S component. The effectiveness of varying the chain section in reducing the pitch motions was found to be limited, similar to the findings for heave motions and roll. Notably, in the hinged configuration, up to four times higher maximum values were recorded when compared to the rigid configuration. Note that these values were obtained for each floating body.

The environmental conditions that led to the highest yaw motions were S wind and NE waves, although most oblique wave directions yielded similar results. Maximum yaw values are severely diminished by the weight of the mooring chains. Chain 1 registered the highest yaw values, with a maximum of 9° for the rigid configuration. Chain 2 reduced the maximum yaw motions with respect to Chain 1 by 33% in the rigid configuration and by 75% in the hinged configuration (Fig. 9). Chain 3 limited this motion by 54% in the rigid configuration and by 75% in the hinged configuration. These yaw motions affect energy yield of FPV systems, since they deviate the PV modules from their ideal alignment.

In terms of yaw motions, the flexible configuration may be more advantageous. The hinged configuration reduced maximum yaw motions by 32% for Chain 1, by 76% for Chain 2 and by 62% in Chain 3. This reduction in yaw motions can positively impact the energy yield of the FPV system. However, it is important to note that the opposite holds true for pitch motions. The hinged configuration, while effective in reducing yaw motions, also results in an increase in pitch motions. These pitch motions can lead to deviations in the ideal tilt of the PV panels, which can negatively affect the energy yield. Therefore, a careful consideration of the trade-offs between yaw and pitch motions is necessary when selecting the FPV configuration for optimal productivity.

As for the overall environmental forces acting on the floating structure, they can be divided into wind induced forces (due to the contribution of drag and lift forces) and wave induced forces (due to the contribution of Froude-Krylov, radiation and diffraction forces). The maximum environmental forces on the floating structure with respect from its CoG as well as the test case that led to them, are presented in Table 6. These correspond to the rigid configuration. The maximum wind forces and moments were registered when the wind was coming from the S, as expected for a higher lift coefficient in this direction. The maximum wave force was registered for side waves (E and W directions) since that is the most exposed direction from the perspective of the floating system. As expected, the highest wave height yielded the highest results.

3.2. Structural analysis

3.2.1. Mooring lines

The maximum forces on the mooring lines for extreme wave conditions are presented in Fig. 10. Each mooring line supports tension when it restrains a particular motion of the floating structure. Depending on the distance each fairlead moves away or towards its anchorage point, some lines tighten while others loose. The rigid configuration shows overall higher mooring force values.

As for chain sections, a sharp increase in the mooring forces was registered for Chain 1. This is due to instantaneous peak loading which, in the case of the rigid configuration, surpasses the breaking load limit (Table 7). These values are dangerously close to the breaking load limit in the hinged configuration. Moreover, even if the lightest mooring line could survive the loads, a slightly heavier mooring line would spare the floating structure from unnecessary loading. Since the forces in Chain 2 and Chain 3 are similar, it can be concluded that adopting Chain 3 would result in an oversized mooring system. Therefore, Chain 2 proves to be the most suitable chain section for this design from a structural standpoint. Given the weight of the selected mooring line, the use of synthetic rope or elastic cables should be studied in future works, from both a structural and productivity perspective. The maximum values were registered in the same scenarios responsible for the maximum surge motions: winds and waves aligned and coming from the S (for M1 and M4) or from the N (for M2 and M3).

An example of peak loading in Chain 1 can be seen in Fig. 11. The heavier chain sections display a harmonic behaviour, with mooring forces oscillating below 5 kN. However, for the lighter chain section, several force peaks or snaps are detected.

3.2.2. FPV components

The results of the hydrodynamic response analysis were the inputs of the structural analysis that was performed through a static FEM approach for every time step of the evaluated test cases. This analysis was performed for Chain 2, since it was proven to be the most suitable in the previous section. The results were stresses in the different structural components of the device, that are to be compared with the mechanical properties of the materials that make them up.

An example of the Von Misses stress in the floats for a particular test case and time step are shown in Fig. 12 as an example. In this case, the stress on the floats is directly related to the hydrodynamic pressure on the cylinders. The stress pattern the floats display means that the structure is currently in the wave through. The extreme cylinders are completely supported by the water, while the middle cylinders are partially surfaced (note that the wavelength is greater that the length of the FPV plant).

The influence of the wave direction on the beam elements is shown, for two periods of the oncoming waves, in Fig. 13. Due to the harmonic nature of the analysed waves, this pattern repeats itself throughout the full simulation, after the ramping process. The waves coming from the N yielded the highest values of stress and showed a greater amplitude of variation and stress gradient. This was the expected result, considering the alignment of the beams with respect to the wave front. Several peaks can be observed in a full cycle. These correspond with the instances the plant is required to rotate to overcome or dismount a crest, resulting in an uneven support by the water.

The highest peak occurs because, once per cycle, an extreme float becomes partially suspended, resulting on a high bending moment on the beam at the position of the next floater, which is completely supported (Fig. 14). On the other hand, when the wave front was coming from the W, a close to constant value of maximum stress was obtained, which also resulted in the lowest stress level. The alignment of the wave front with the beams ensured a constant support, which resulted in reduced stresses. A middle ground between both scenarios was found when waves were approaching the structure form the SW.

The structural verification of the main components, as well as the test cases that led to them, are presented in Table 8. This maximum values were obtained for the rigid configuration.

The stress on the floats was obtained through the von Misses yield criterion. The maximum stress values were reached for the wave front perpendicular to the panels, but oblique wave fronts yielded similar results. Most of the stress was circumferential, due to the pressure of the PV panels that sit on the floating system as well as the hydrostatic and hydrodynamic pressures acting on the cylinders. Some axial stress was

Table 6
Maximum environmental loads on the FPV platform and corresponding test conditions.

Type	Loads	Test conditions				
	(kN or kNm)	U (m/s)	θ	H (m)	T (s)	δ
Wind force	9	30	S	1	7	S
Wind momentum	73	30	S	1	7	S
Wave force	326	30	N	1	7	E
Wave momentum	2787	30	N	1	7	NE

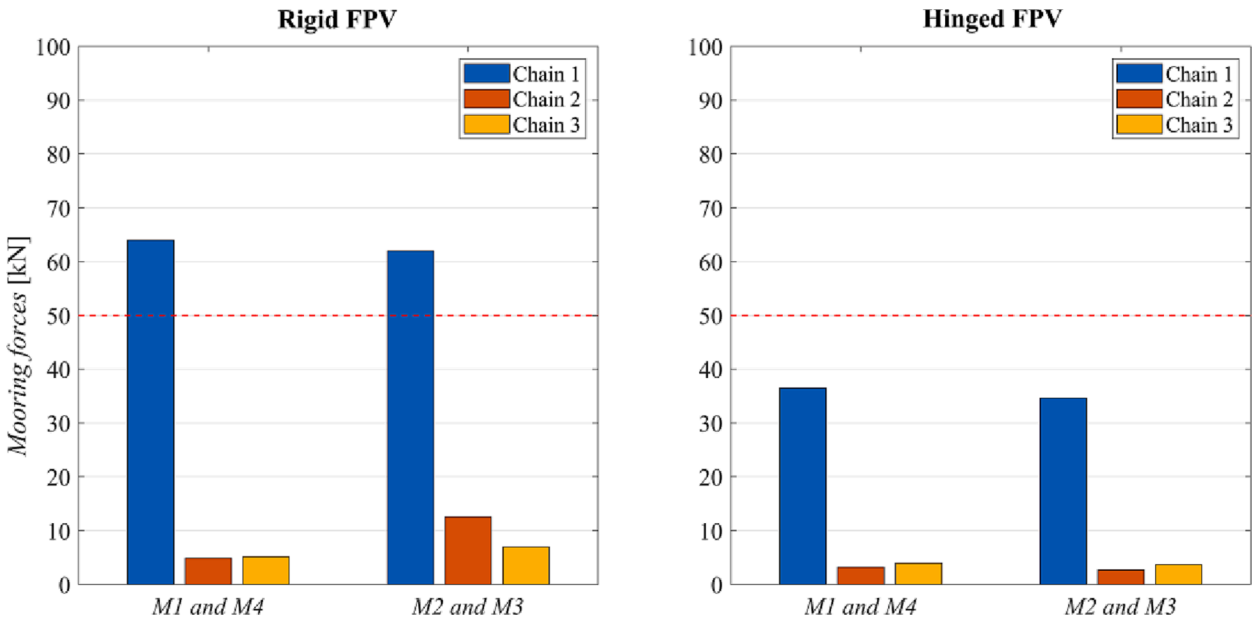

Fig. 10. Maximum mooring forces for $H = 1$ m. The red dotted line represents the breaking load of Chain 1.

Table 7
Initial forces, maximum forces and safety factor for the studied chain sections.

Configuration	Chain section	Initial tensile force (kN)	Maximum tensile force (kN)	Safety factor
Rigid	1	0.5	64.2	0.78
Rigid	2	1.1	12.6	10.48
Rigid	3	2.2	7.1	35.35
Hinged	1	0.5	36.5	1.37
Hinged	2	1.1	3.2	41.25
Hinged	3	2.2	3.7	67.84

also registered due to the wave pressure exerted on the flat end caps of the floating cylinders. Deformations were very small (<1 cm). However, since external forces caused compression stresses, a buckling collapse analysis may be required. A very high safety factor is reached, which means that the limiting design factor for this floating system could be related to material degradation or punching shear loads.

The maximum stresses on the beams were registered for the wave directions aligned with them. Note that, due to the size of the plant and the slope of the analysed waves, at no time is a floater fully suspended. This results in low bending loads since the main gravitational loads rest directly in the floating system. The maximum axial stresses were reached due to a combination of bending moments and axial forces. Deformations were very small (<0.5 cm) Safety factors are quite high, which means these beams have a margin for structural optimization for the considered environmental conditions. Cheaper, less resistant alternatives to FRP should be studied, bearing corrosion resistance and weight in mind. Shear stresses were overall small.

4. Conclusions

This study proposed a comprehensive design methodology for evaluating floating photovoltaic (FPV) structures subjected to environmental conditions, particularly wind and waves, from hydrodynamic and structural perspectives. The methodology was applied to a Class 1

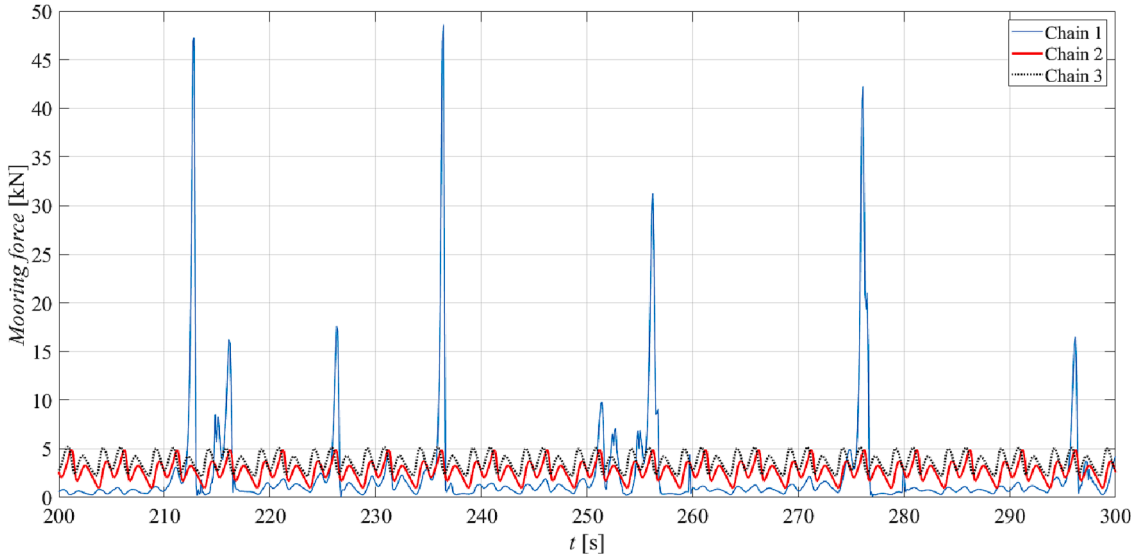

Fig. 11. Forces on mooring line M1 for the rigid configuration (environmental conditions: $H = 1$ m, $T = 5$ s, $U = 30$ m/s, $\theta = S$ and $\delta = S$).

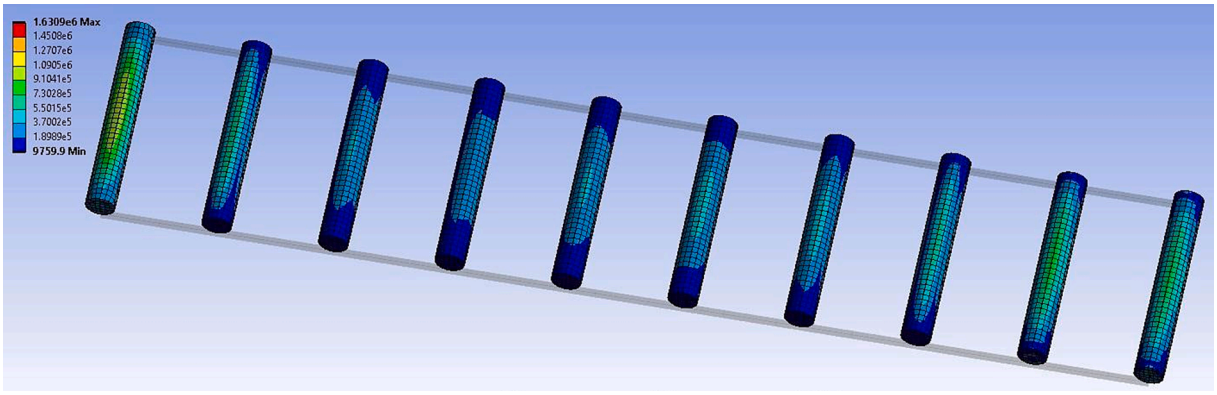

Fig. 12. Von Misses stress in the cylindres of the rigid configuration, (environmental conditions: $H = 1$ m, $T = 5$ s, $U = 0$ m/s and $\delta =$ N).

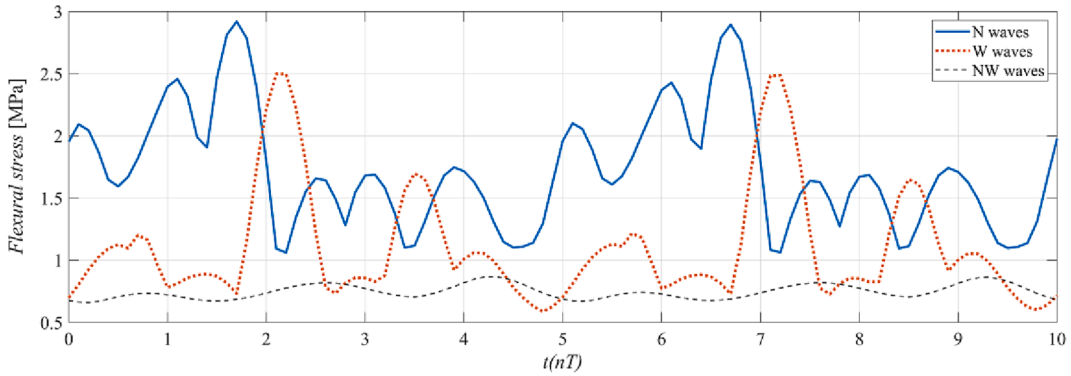

Fig. 13. Influence of wave direction on the maximum stress measured in the beam elements of the rigid configuration (environmental conditions: $H = 1$ m, $T = 5$ s, $U = 30$ m/s and $\delta =$ N).

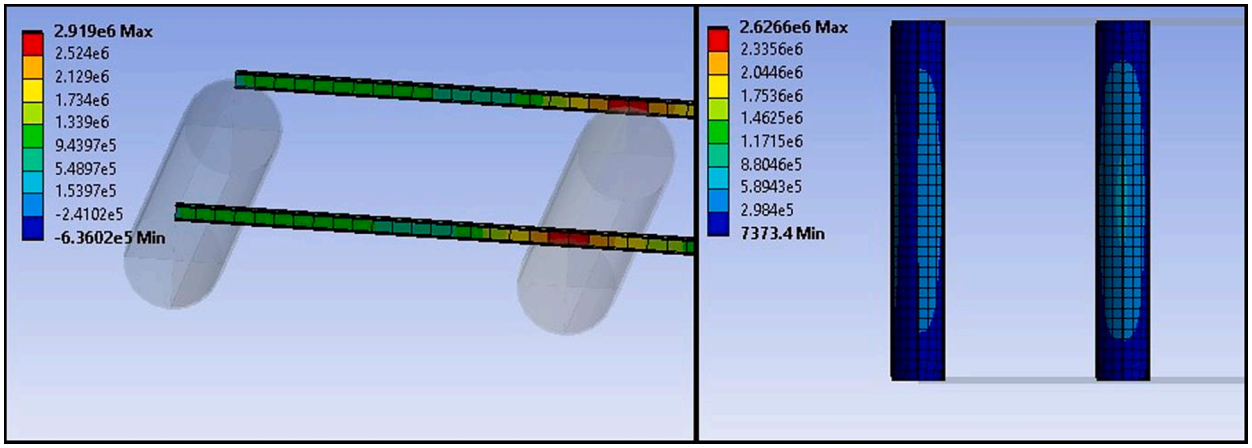

Fig. 14. Maximum bending stress in the beams (environmental conditions: $H = 1$ m, $T = 5$ s, $U = 30$ m/s, $\theta =$ N and $\delta =$ N).

Table 8
Structural verification of the main components of the FPV plant.

Component	Verification	Maximum value	Safety factor	Test conditions				
				U	θ	H (m)	T (s)	δ
Floats	Von Misses (MPa)	3.1	10.64	30	N	1	5	N
Beams	Flexion – axial(MPa)	2.9	143.21	30	N	1	5	N
Beams	Shear – torsion (MPa)	0.5	146.60	30	N	1	5	N

pontoon-type structure with two configurations: rigid and hinged. A total of 558 simulations were conducted, combining various environmental actions, configurations, and mooring line chain sections, providing essential data on loads and motion time series for subsequent structural analysis. Although the methodology was implemented in Ansys Mechanical and Aqwa software, other finite element method (FEM) and boundary element method (BEM) solvers could be utilized.

The analysis revealed that wind forces primarily influenced surge and sway motions, while wave forces played a dominant role in other motion components. Comparing the hinged configuration to the rigid one, a significant reduction in the maximum yaw motions ranging from 32% to 76% was observed, depending on the chain section employed. This reduction in yaw motions positively impacted the energy yield. However, an inverse trend was observed for pitch motions, which could potentially impact the optimal tilt of PV panels and their energy yield. Hence, a comprehensive assessment of wave-induced motions is crucial for selecting the optimal FPV configuration.

Furthermore, heavier chain sections effectively limited surge, sway, and yaw motions, with variations of up to 75% observed in the hinged configuration when comparing different chain options. Careful selection and optimization of the chain weight are important for minimizing yaw motions and maximizing FPV system productivity. The study also identified that the lightest chain section experienced peak loads exceeding its breaking load limit with a safety factor of 0.78, highlighting the need for a heavier mooring line to ensure structural integrity.

Structural analysis indicated that beam elements experienced mainly flexural stresses during wave loading, while the floating systems endured mostly circumferential stresses. Adequate safety factors were observed, but alternative materials with corrosion resistance and weight considerations should be explored. The results emphasized the significance of wave characteristics, mooring system configuration, and overall system flexibility in the successful deployment of FPV systems. Future work should include analysing current loads in addition to wind and wave loads, conducting physical experiments to validate numerical simulations, and integrating energy efficiency assessment into the structural design optimization.

In conclusion, this research contributes valuable insights into the design and performance evaluation of FPV systems. The findings underscore the importance of considering environmental conditions, structural aspects, and energy efficiency in optimizing FPV configurations. The proposed methodology and recommendations for future work serve as a foundation for further advancements in the field of floating photovoltaic structures.

Declaration of Competing Interest

The authors declare that they have no known competing financial interests or personal relationships that could have appeared to influence the work reported in this paper.

Acknowledgments

This work was supported by the PORTOS project co-financed by the Interreg Atlantic Area Programme through the European Regional Development Fund [grant number EAPA_784/2018]. During this work, R. Claus was also supported by the “Programa Severo Ochoa de Ayudas para la investigación y docencia”, a research fellowship programme financed by the Government of the Principality of Asturias (Spain) [grant number AYUD0029T01].

References

[1] Kabir, E., Kumar, P., Kumar, S., Adelodun, A.A., Kim, K.-H., 2018. Solar energy: Potential and future prospects. Renew. Sustain. Energy Rev. 82, 894–900. https://doi.org/10.1016/j.rser.2017.09.094.

[2] Rosa-Clot M, Tina GM. Current Status of FPV and Trends. Float. PV Plants, Academic Press; 2020, p. 9–18.

[3] Turney, D., Fthenakis, V., 2011. Environmental impacts from the installation and operation of large-scale solar power plants. Renew. Sustain. Energy Rev. 15 (6), 3261–3270.

[4] Ueda, Y., Sakurai, T., Tatebe, S., Itoh, A., Kurokawa, K., 2008. Performance Analysis of Pv Systems on the Water. 23rd Eur. Photovolt. Sol. Energy Conf. Exhib. 1–5. https://doi.org/10.4229/23rdEUPVSEC2008-4EP.1.3.

[5] Oliveira-Pinto, S., Stokkermans, J., 2020. Assessment of the potential of different floating solar technologies–Overview and analysis of different case studies. Energy Convers. Manag. 211.

[6] Elminshawy, N.A.S., Osama, A., El-Damhogi, D.G., Oterkus, E., Mohamed, A.M.I., 2021. Simulation and experimental performance analysis of partially floating PV system in windy conditions. Sol. Energy 230, 1106–1121. https://doi.org/10.1016/j.solener.2021.11.020.

[7] Cazzaniga, R., Cicu, M., Rosa-Clot, M., Rosa-Clot, P., Tina, G.M., Ventura, C., 2018. Floating photovoltaic plants: Performance analysis and design solutions. Renew. Sustain. Energy Rev. 81, 1730–1741. https://doi.org/10.1016/j.rser.2017.05.269.

[8] Liu, H., Krishna, V., Lun Leung, J., Reindl, T., Zhao, L.u., 2018. Field experience and performance analysis of floating PV technologies in the tropics. Prog. Photovolt. Res. Appl. 26 (12), 957–967.

[9] Farrar, L.W., Bahaj, A.B.S., James, P., Anwar, A., Amdar, N., 2022. Floating solar PV to reduce water evaporation in water stressed regions and powering water pumping: Case study Jordan. Energy Convers. Manag. 260, 115598 https://doi.org/10.1016/j.enconman.2022.115598.

[10] Haas, J., Khalighi, J., de la Fuente, A., Gerbersdorf, S.U., Nowak, W., Chen, P.J., 2020. Floating photovoltaic plants: Ecological impacts versus hydropower operation flexibility. Energy Convers. Manag. 206. https://doi.org/10.1016/j.enconman.2019.112414.

[11] Farfan, J., Breyer, C., 2018. Combining floating solar photovoltaic power plants and hydropower reservoirs: A virtual battery of great global potential. Energy Procedia 155, 403–411. https://doi.org/10.1016/j.egypro.2018.11.038.

[12] Kaymak, M.K., Şahin, A.D., 2022. The first design and application of floating photovoltaic (FPV) energy generation systems in Turkey with structural and electrical performance. Int. J. Precis. Eng. Manuf. Technol. 9 (3), 827–839.

[13] López, M., Soto, F., Hernández, Z.A., 2022. Assessment of the potential of floating solar photovoltaic panels in bodies of water in mainland Spain. J. Clean. Prod. 340, 130752 https://doi.org/10.1016/j.jclepro.2022.130752.

[14] Hooper, T., Armstrong, A., Vlaswinkel, B., 2021. Environmental impacts and benefits of marine floating solar. Sol. Energy 219, 11–14. https://doi.org/10.1016/j.solener.2020.10.010.

[15] Golroodbari, S.Z.M., Vaartjes, D.F., Meit, J.B.L., van Hoeken, A.P., Eberveld, M., Jonker, H., van Sark, W.G.J.H.M., 2021. Pooling the cable: A techno-economic feasibility study of integrating offshore floating photovoltaic solar technology within an offshore wind park. Sol. Energy 219, 65–74.

[16] Temiz, M., Dincer, I., 2021. Techno-economic analysis of green hydrogen ferries with a floating photovoltaic based marine fueling station. Energy Convers. Manag. 247, 114760 https://doi.org/10.1016/j.enconman.2021.114760.

[17] Cazzaniga R. Chapter 4 - Floating PV Structures. In: Rosa-Clot M, Marco Tina G, editors. Float. PV Plants, Academic Press; 2020, p. 33–45. doi:https://doi.org/10.1016/B978-0-12-817061-8.00004-X.

[18] Claus, R., López, M., 2022. Key issues in the design of floating photovoltaic structures for the marine environment. Renew. Sustain. Energy Rev. 164.

[19] DNV GL AS. DNVGL-RP-0584: Design, development and operation of floating solar photovoltaic systems. 2021.

[20] Oliveira-Pinto, S., Stokkermans, J., 2020. Marine floating solar plants: An overview of potential, challenges and feasibility. Proc. Inst. Civ. Eng. Marit. Eng. 173, 120–135. https://doi.org/10.1680/jmaen.2020.10.

[21] Al-Yacouby, A.M., Halim, E.R.B.A., Liew, M.S., 2020. Hydrodynamic Analysis of Floating Offshore Solar Farms Subjected to Regular Waves. Adv. Manuf. Eng., Springer 375–390.

[22] Mursid, O., Malau, K.R., Huda, N., Abidin, A.M.A., Sutarno, G., 2021. Design and Feasibility Studies A Floating Photovoltaic to Supply Electricity for Isolated Island Village in Indonesia. IOP Conf. Ser. Earth Environ. Sci. 698 (1), 012033.

[23] Ikhennicheu, M., Danglade, B., Pascal, R., Arramounet, V., Trébaol, Q., Gorintin, F., 2021. Analytical method for loads determination on floating solar farms in three typical environments. Sol. Energy 219, 34–41.

[24] Kim, S.H., Baek, S.C., Choi, K.B., Park, S.J., 2020. Design and installation of 500-kW floating photovoltaic structures using high-durability steel. Energies 13. https://doi.org/10.3390/en13194996.

[25] DNV GL. DNVGL-CG-0130: Wave loads. 2018. doi:10.1201/b15120-2.

[26] DNV AS. DNV-RP-C205: Environmental conditions and environmental loads 2019.

[27] You, J., Lim, M., You, K., Lee, C., 2021. Wind Coefficient Distribution of Arranged Ground Photovoltaic Panels. Sustainability 13. https://doi.org/10.3390/su13073944.

[28] Mignone, A., Inghirami, G., Rubini, F., Cazzaniga, R., Cicu, M., Rosa-Clot, M., 2021. Numerical simulations of wind-loaded floating solar panels. Sol. Energy 219, 42–49. https://doi.org/10.1016/j.solener.2020.11.079.

[29] Bei Y, Yuan B, Wu Q. Numerical Simulation of Wind Load Characteristics of Floating Photovoltaics. 2022 5th Int. Conf. Energy, Electr. Power Eng., 2022, p. 1104–8.

[30] Choi, S.M., Lee, G.R., Park, C.D., Cho, S.H., Lim, B.J., 2021. Wind load on the solar panel array of a floating photovoltaic system under extreme hurricane conditions. Sustain. Energy Technol. Assess. 48, 101616 https://doi.org/10.1016/j.seta.2021.101616.

[31] Choi, S.M., Park, C.D., Cho, S.H., Lim, B.J., 2023. Effects of various inlet angle of wind and wave loads on floating photovoltaic system considering stress distributions. J. Clean. Prod. 387, 135876 https://doi.org/10.1016/j.jclepro.2023.135876.
[32] Yu, F., Su, Y., Liu, Y., Liu, H., Duan, F., 2021. Dynamic response of the mooring system in the floating photovoltaic power station. J. Phys. Conf. Ser. 2087, 12028.
[33] Claus, R., Cebada, A., Fernández, S., López, M., 2022. Structural analysis of a floating photovoltaic plant in the marine environment. 5th Iber. Conf. Struct. Integr.
[34] Kanotra, R., Shankar, R., 2022-Chennai,. Floating Solar Photovoltaic Mooring System Design and Analysis. Ocean. 2022, 1–9.
[35] Ikhennicheu, M., Blanc, A., Danglade, B., Gilloteaux, J.-C., 2022. OrcaFlex Modelling of a Multi-Body Floating Solar Island Subjected to Waves. Energies 15 (23), 9260.
[36] Magkouris, A., Belibassakis, K., Rusu, E., 2021. Hydrodynamic Analysis of Twin-Hull Structures Supporting Floating PV Systems in Offshore and Coastal Regions. Energies 14, 5979.
[37] Bugeja, R., Mule' Stagno, L., Branche, N., 2021. The effect of wave response motion on the insolation on offshore photovoltaic installations. Sol Energy Adv 1, 100008.
[38] López, M., Claus, R., Soto, F., Cebada, A., Hernández, Z., 2021. Structural reliability of a novel offshore floating photovoltaic system to supply energy demands of ports. 8th Int. Conf. Mar. Struct., Trondheim.
[39] Yang, R.-Y., Yu, S.-H., 2021. A Study on a Floating Solar Energy System Applied in an Intertidal Zone. Energies 14, 7789.
[40] Kim, S.-H., Yoon, S.-J., Choi, W., 2017. Design and construction of 1MW class floating PV generation structural system using FRP members. Energies 10 (8), 1142.
[41] Hayibo, K.S., 2021. Quantifying the Value of Foam-Based Flexible Floating Solar Photovoltaic Systems. Michigan Technological University.
[42] Nagananthini, R., Nagavinothini, R., Balamurugan, P., 2020. Floating Photovoltaic Thin Film Technology—A Review. Intell. Manuf. Energy Sustain. 329–338.
[43] Ravichandran, N., Ravichandran, N., Panneerselvam, B., 2022. Comparative assessment of offshore floating photovoltaic systems using thin film modules for Maldives islands. Sustain. Energy Technol. Assess. 53, 102490 https://doi.org/10.1016/j.seta.2022.102490.
[44] Sree, D.K.K., Law, A.-K., Pang, D.S.C., Tan, S.T., Wang, C.L., Kew, J.H., Seow, W.K., Lim, V.H., 2022. Fluid-structural analysis of modular floating solar farms under wave motion. Sol. Energy 233, 161–181.
[45] Lee, Y.G., Joo, H.J., Yoon, S.J., 2014. Design and installation of floating type photovoltaic energy generation system using FRP members. Sol. Energy 108, 13–27. https://doi.org/10.1016/j.solener.2014.06.033.
[46] Dai, J., Zhang, C., Lim, H.V., Ang, K.K., Qian, X., Wong, J.L.H., Tan, S.T., Wang, C. L., 2020. Design and construction of floating modular photovoltaic system for water reservoirs. Energy 191. https://doi.org/10.1016/j.energy.2019.116549.
[47] Xu, P., Wellens, P.R., 2022. Theoretical analysis of nonlinear fluid–structure interaction between large-scale polymer offshore floating photovoltaics and waves. Ocean Eng. 249, 110829 https://doi.org/10.1016/j.oceaneng.2022.110829.
[48] Xu, P., Wellens, P.R., 2022. Fully nonlinear hydroelastic modeling and analytic solution of large-scale floating photovoltaics in waves. J. Fluids Struct. 109, 103446 https://doi.org/10.1016/j.jfluidstructs.2021.103446.
[49] Newman, J.N., Lee, C.-H., 2002. Boundary-element methods in offshore structure analysis. J. Offshore Mech. Arct. Eng. 124, 81–89.
[50] Chakrabarti, S.K., 1987. Hydrodynamics of offshore structures. WIT press.
[51] Le Méhauté, B., 2013. An introduction to hydrodynamics and water waves. Springer Science & Business. Media.
[52] Morison, J.R., Johnson, J.W., Schaaf, S.A., et al., 1950. The force exerted by surface waves on piles. J. Pet Technol. 2, 149–154.
[53] Liu, L., Sun, J., Chen, W., Sun, P., 2017. Study on the machining distortion of aluminum alloy parts induced by forging residual stresses. Proc. Inst. Mech. Eng. Part B J. Eng. Manuf. 231 (4), 618–627.
[54] Kaymak, M.K., cSahin, AD., 2022. Floating and terrestrial photovoltaic systems comparison under extreme weather conditions. Int. J. Energy Res. 46, 20719–20727.
[55] Awad A, El Gamasy R, Abd El Wahab A, Abdellatif MH. Mechanical and Physical Properties of PP and HDPE. Eng Sci 2019.
[56] Trillo - Anclas y Cadenas n.d. https://www.rtrillo.com/es/inicio/ (accessed June 20, 2019).
[57] Cebada-Relea, A.J., López, M., Aenlle, M., 2022. Time-domain numerical modelling of the connector forces in a modular pontoon floating breakwater under regular and irregular oblique waves. Ocean Eng. 243, 110263 https://doi.org/10.1016/j.oceaneng.2021.110263.
[58] ANSYS. Aqwa Theory Manual 2021.